On the Propagation of Viscous Wakes and Potential Flow in Axial-Turbine Cascades

T. Korakianitis
Assistant Professor of Mechanical Engineering,
Washington University,
St. Louis, MO 63130

This paper investigates the propagation of pressure disturbances due to potential-flow interaction and viscous-wake interaction from upstream blade rows in axial-turbine-blade rotor cascades. Results are obtained by modeling the effects of the upstream stator viscous wake and potential-flow fields as incoming disturbances on the downstream rotor flow field, where the computations are performed. A computer program is used to calculate the unsteady rotor flow fields. The amplitudes for the rotor inlet distortions due to the two types of interaction are based on a review of available experimental and computational data. We study the propagation of the isolated potential-flow interaction (no viscous-wake interaction), of the isolated viscous wake interaction (no potential-flow interaction), and of the combination of interactions. The discussion uses as example a lightly loaded cascade for a stator-to-rotor-pitch ratio R = 2. *We examine the relative magnitudes of the unsteady forces for two different stator-exit angles. We also explain the expected differences when the stator-to-rotor pitch ratio is decreased (to* R = 1*) and increased (to* R = 4*). We offer new and previously unpublished explanations of the mechanisms of generation of unsteady forces on the rotor blades. The potential flow field of the rotor cuts into the potential flow field of the stator. After the potential-flow disturbance from the stator is cut into a rotor cascade, it propagates into the relative flow field of the rotor passage as a potential-flow disturbance superimposed on the rotor-relative flow. The potential flow field of the rotor near the leading edge and the leading edge itself cut into the wake and generate two counterrotating vortical patterns flanking the wake centerline in the passage. The vortical pattern upstream of the wake centerline generates an increase in the local pressure (and in the forces acting on the sides of the passage). The vortical pattern downstream of the wake centerline generates a decrease in the local pressure (and in the forces acting on the sides of the passage). The resulting unsteady forces on the blades are generated by the combined (additive) interaction of the two disturbances.*

Introduction

In the preliminary design of turbines, one starts for two dimensional stator and rotor velocity diagrams at one or more radii across the blade span and proceeds to design the shape of the two-dimensional cascades of the rotor and the stator. There is a lot of freedom on the choice of the ratio of the number of rotor blades to the number of stator blades, which affects the pitches S_{rb} and S_{sb} and is equal to the stator-to-rotor-pitch ratio R, defined by:

$$R \equiv \frac{S_{sb}}{S_{rb}} = \frac{N_{rb}}{N_{sb}} \tag{1}$$

The effect of R on geometry is illustrated in Fig. 1, where the geometry of the downstream rotor is kept constant, the non-

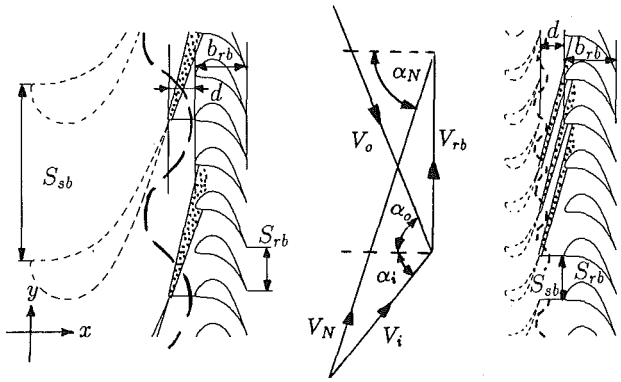

$R = S_{sb}/S_{rb} = 4.0$ $\qquad$ $R = S_{sb}/S_{rb} = 1.0$

Fig. 1 The effect of R on the stage geometry. The rotor velocity diagrams and the downstream rotors (flow from left to right) are identical.

Contributed by the International Gas Turbine Institute and presented at the 36th International Gas Turbine and Aeroengine Congress and Exposition, Orlando, Florida, June 3-6, 1991. Manuscript received at ASME Headquarters March 4, 1991. Paper No. 91-GT-373. Associate Technical Editor: L. A. Riekert.

dimensional geometry of the upstream stator is identical, but R is varied by changing the value of S_{sb}. The two-dimensional flow unsteadiness between the rotor and the stator is due to: viscous velocity wakes shed from the trailing edge of the stator, generated by the boundary layer along the stator surfaces; inviscid potential-flow interaction because of the relative motion of the lifting surfaces of the rotor and the stator; vortices shed at the stator trailing edge; flutter of both cascades; and the effect of flow changes due to cooling flows in high-pressure high-temperature turbine stages. In Fig. 1 the velocity wake is illustrated in the dotted region starting at the stator trailing edges; the potential-flow interaction is illustrated as a sinusoidal static-pressure variation with a maximum at the stator trailing edge. As R increases, the potential-flow interaction relative to the rotor increases, and its frequency and decay rate decrease. As R increases, the amplitude of the velocity defect in the wake remains about constant, and one may observe a modest increase in the width of the wake because of the increased Reynolds numbers and larger lengths over which the boundary layers develop on the larger stators.

Engine designers try to "detune" the forced response of the cascades by choosing unequal numbers of blades in stators and rotors N_{sb} and N_{rb}. Economic considerations force designs to higher values of R, but this results in larger disturbances entering the rotor cascade and it will probably lead to larger unsteady forces acting on the rotor. For a given rotor size and velocity diagrams R is inversely proportional to the reduced frequency parameter, defined by:

$$\tilde{\omega} \equiv \frac{\omega \cdot b_{rb}}{c_x} = \frac{2\pi V_{rb}\, b_{rb}}{S_{rb}\, c_x} \cdot \frac{1}{R} \tag{2}$$

The purpose of this paper is to provide some insights on the magnitude and shape of the unsteady forcing function acting on the blade structure, and to examine some of the mechanisms by which these forces are generated in the rotor passages.

Background

In past investigations (Korakianitis, 1987a, 1988a, 1988b, 1988c, 1992a, 1992b) we computed the amplitude of the harmonics of the spatially analyzed unsteady forces on rotor blades as a function of R for a series of typical turbine cascades. For a first approximation we considered the effect of the viscous wake interaction (generated by the boundry layers along the blade surfaces and propagating downstream only) and of the potential flow interaction (a static-pressure variation due to the presence of the lifting surfaces in the cascades and propagating upstream as well as downstream). We neglected the effect of vortex shedding and assumed infinitely rigid blades without cooling slots that expel lower-enthalpy jets of cooling air. For these studies (past and the present one) we have used Giles' (1988a) computer program UNSFLO (which models the two-dimensional, unsteady, compressible, inviscid flow around rotor blades) to compute the flow field and the forces for different stator-exit (nozzle) angles α_N. This program was chosen because it can handle arbitrary values of R with reasonable CPU and storage requirements due to a novel "tilting" of the time domain. In the computational field the problem has been simplified by considering the effects of the stator disturbances on the rotor blades in the rotor-relative frame.

The accuracy of the computations has been checked in the past by Giles (1988a) and Korakianitis (1987a, 1988b, 1992a). These checks involved comparisons of the results of calculations using UNSFLO with the results of four steady and unsteady-flow cases of known theoretical or experimental output. For steady flows we used a comparison of computed results with the closed-form analytic solution obtain by conformal transformation for the incompressible potential flow past Gostelow's (1984) compressor cascade (Korakianitis, 1987a, 1988b, 1992a). For unsteady flows three checks have been published. Giles (1988a) published comparisons with the theoretical results of a sinusoidal wake acting on a flat-plate compressor cascade, and comparisons with measurements and computations performed on a turbine cascade by Hodson (1983, 1985a, 1985b). Korakianitis (1987a, 1988b, 1992a) also compared computational results with the experimental data obtained with laser two-focus velocimeter measurements in a rotor cascade operating behind a stator at the DLR (Binder et al., 1987).

This paper examines the propagation of the same disturbances, of the viscous wake and the potential-flow interaction, as a typical rotor cascade moves past one stator pitch by examining details of the flow fields at six relative positions of rotors and stator disturbances. At the same time we match

Nomenclature

a = acoustic velocity (Eq. (4))
B = amplitude of potential variation (Eq. (6))
b = axial chord
C_L = tangential-lift coefficient (Eq. (10))
c = rotor-inlet total sonic velocity (Eq. (11))
D = wake amplitude, fraction of V_N (Eq. (3))
d = stator-rotor axial gap (fraction of b_{rb})
F', F = force (Eq. (11))
$j \equiv \sqrt{-1}$ (Eq. (5))
M = Mach number
N = number of blades (Eq. (1))
$R \equiv S_{sb}/S_{rb}$ = stator-to-rotor-pitch ratio
S = pitch of a cascade
T_z', T_z = moment (in the z direction) (Eq. (11))
t = time (nondimensionalized by y/S_{sb})
u = velocity component in the x direction
V = velocity
V_{ip} = velocity perturbation due to potential, fraction of c (Eq. (7))
v = velocity component in the y direction
W = characteristic width of the wake, expressed as fraction of S_{sb} (Eq. (3))
(x, y, z) = Cartesian coordinates (in subscripts also)
α = flow angle
$\Delta\epsilon$, ϵ = angles locating the potential (Eqs. (7), (8))
δ = perturbation operator (on u and v)
ξ = parameter for the x decay of Φ (Eq. (6))
ρ = relative total density at rotor inlet
Φ = velocity potential defined by Eq. (5)
ω = rotor passing frequency (Eq. (2))
$\tilde{\omega}$ = reduced frequency parameter (Eq. (2))

Subscripts

i,o = rotor-relative inlet, outlet, respectively
ip = flow property for potential-flow model
iw = flow property in the wake
N = stator-exit (nozzle, in absolute frame)
p = pressure side
q = suction (s) or pressure (p) side (Eq. (3))
rb = rotor blade row
s = suction side
sb = stator blade row
ss = steady flow

observations of details of the flow fields with the shape of the forcing function.

The Rotor-Inlet Boundary

Results have been obtained by considering the two disturbances from the upstream stator (viscous wake and potential-flow interaction) as inputs to the computational rotor-inlet boundary. The rotor-relative flow is computed; the stator disturbances are modeled and input as inlet distortions moving across the computational rotor-inlet boundary.This simplification provides accurate computational results only if one is extremely careful to specify the correct boundary conditions to the problem. Details of the following derivations have been published by Korakianitis (1987a, 1992) and Giles (1988b). A few important equations have been included here for clarity and completeness because they are essential to understanding the model of the rotor-inlet boundary, and the following results and discussion.

The axial gap between blade rows in modern engines is between 0.2 and 0.5 of the axial chord. Narrower gaps result in shorter engines but increase the unsteadiness to which the next blade row is subjected. Throughout these investigations we have used $d=0.3$, nondimensionalized with the rotor axial chord b_{rb}.

The velocity disturbance is characterized by the maximum amplitude of the velocity defect D, expressed as a fraction of the undisturbed velocity, and by the "width" W of the velocity defect (see Eq. (3)). Most velocity wakes observed in experimental data have velocity distributions which resemble Gaussian distributions. The width of the velocity defect is characterized by the corresponding characteristic width of the Gaussian distribution that would best fit the velocity data. In the following this width is expressed as a fraction of the pitch of the blade cascade that generates the wake. In most cases the pressure side of the velocity wake is narrower than the suction side, especially for small axial distances downstream of the cascade that generates the wake. The reason for this is that the boundary layer of the pressure side is thinner than the boundary layer of the suction side. Two "characteristic widths" are used: the suction-side characteristic width, and the pressure-side characteristic width. For the wake model we assumed that in the stator frame the flow vectors in the wake are parallel to the undisturbed flow (a velocity deficit with no angle variation), that the static pressure is constant across the wake, that the total enthalpy is constant across the wake, and that the velocity defect is an asymmetric Gaussian distribution. The above are modeled by:

$$u_{iw,q}=V_N\left[1-D\cdot\exp\frac{1}{2}\left(-\frac{y-\tan(\alpha_N)}{S_{sb}W_q}\right)^2\right]\cos(\alpha_N)$$
$$v_{iw,q}=V_N\left[1-D\cdot\exp\frac{1}{2}\left(-\frac{y-\tan(\alpha_N)}{S_{sb}W_q}\right)^2\right]\sin(\alpha_N) \quad (3)$$

where q is either s (for the suction surface) or p (for the pressure surface). The way this wake function varies from one computational rotor passage to the next, and a literature review of experimental data on wake amplitudes and widths has been published (Korakianitis, 1988a, 1992a). Based on these data we chose as a representative wake amplitude $D=0.10$ of V_N, and characteristic widths $W_p=0.14$ and $W_s=0.16$ of the rotor pitch S_{rb} for the axial gap $d=0.30$.

The model for the potential-flow disturbance was developed by observing the experimentally measured and computed static pressure fields of various turbine-blade cascades. These indicate that across the line of the trailing edges of the cascades there is a variation of static pressure with maxima at (or very near) the trailing edges and minima at (or very near) the middle of the passage. The exact location and shape of the pressure variation depends on the geometric shape of the passage. The pressure variation is nearly sinusoidal and the amplitude of the pressure disturbance decays very fast with distance downstream. Numerous examples of this static pressure variation can be seen in the experimental wake sources (Korakianitis, 1987a, 1988a, 1992a). For example, measured cascade data such as those shown in Fig. 6 of Sieverding et al. (1984), Fig. 7 of Boletis and Sieverding (1984), Fig. 6 of Sonoda, (1985), and Fig. 4 of Yamamoto and Yanagi (1985), show the shape and the rapid decay of the potential-flow interaction.

The potential-flow model (in the stator frame) is derived as a two-dimensional, linear, isentropic, irrotational perturbation to uniform flow (see page 198 of the text by Liepmann and Roshko, 1957):

$$(u^2-a^2)\frac{\partial u}{\partial x}+(v^2-a^2)\frac{\partial v}{\partial y}+uv\left(\frac{\partial u}{\partial y}+\frac{\partial v}{\partial x}\right)=0 \quad (4)$$

The velocity potential is defined by:

$$\frac{\partial\Phi}{\partial x}\equiv u \qquad \frac{\partial\Phi}{\partial y}\equiv v \quad (5)$$

For subsonic flows of interest to this study one expects that the potential-flow interaction is periodic in the y direction and that it decays exponentially in the x direction. Thus the general solution of Eq. (4) is of the form:

$$\Phi(x,y)=B\cdot\exp\left[j\frac{2\pi}{S_{sb}}y+\xi x\right] \quad (6)$$

where B is the amplitude, ξ governs the decay and $2\pi/S_{sb}$ dictates the periodicity of the potential Φ. Substituting these in Eq. 4 we derive solutions of the form:

$$\delta v=-V_{ip}\cdot\exp\left[-\frac{2\pi}{S_{sb}}\frac{\sqrt{1-M^2}}{1-M_x^2}(x-x_{inl})\right]\cdot\sin[2\pi(\epsilon+\Delta\epsilon)] \quad (7)$$

$$\delta u=-\tan(\alpha_{ip})\delta v-\frac{\sqrt{1-M^2}}{1-M_x^2}V_{ip}\cdot\exp\left[-\frac{2\pi}{S_{sb}}\frac{\sqrt{1-M^2}}{1-M_x^2}(x-x_{inl})\right]\cdot\cos[2\pi(\epsilon+\Delta\epsilon)]$$

where M is given by $M=\sqrt{M_x^2+M_y^2}$, the phase ϵ at any location is given by

$$\epsilon=\frac{y-\tan(\alpha_{ip})x}{S_{sb}}, \quad (8)$$

$\tan(\alpha_{ip})$ is the direction of propagation of the potential field given by

$$\tan(\alpha_{ip})=-\frac{M_xM_y}{1-M_x^2}, \quad (9)$$

and V_{ip} is the maximum perturbation in v at the stator trailing edge (rotor-inlet) boundary (a fraction of c). Then the velocity perturbations are a function of the axial distance from the inlet boundary $(x-x_{inl})$, where x_{inl} denotes the axial location of the computational rotor-inlet boundary and $\Delta\epsilon$ is a phase-shifting constant used to ensure that the maximum amplitude in the pressure disturbance due to the potential-flow field of the stator coincides with the centerlines of the velocity wakes at the (x_{inl}, y) locations that model the stator trailing edges.

The amplitude of V_{ip} was chosen by investigating the pressure and velocity fluctuations from experimental measurements and from published computations across the line joining the trailing edges of numerous typical turbine-stator cascades, and across other lines a little downstream (5 and 10 percent of the axial chord) parallel to the line across the trailing edges. These measurements indicated that across the line of the trailing edges the

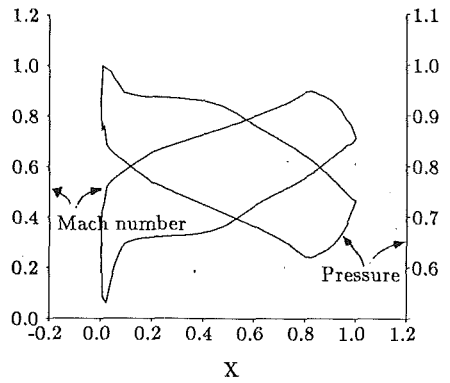

Fig. 2(*a*) Surface Mach number and pressure distributions

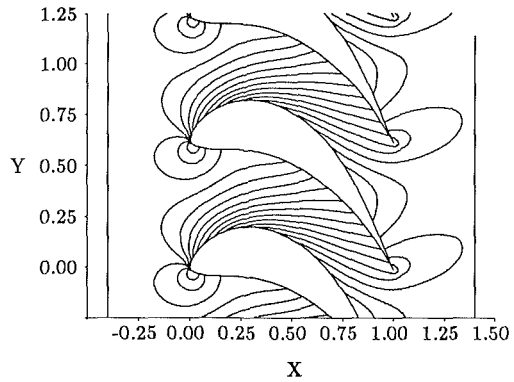

Fig. 2(*b*) Passage pressure distribution (increment 0.02)

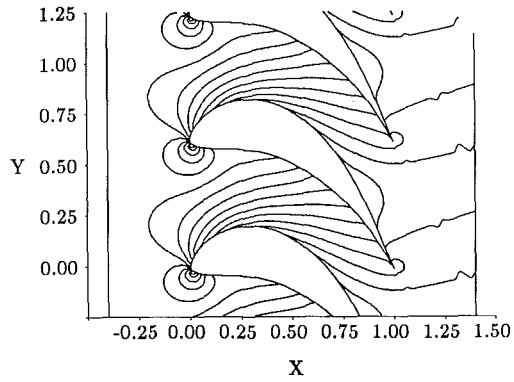

Fig. 2(*c*) Passage Mach number distribution (increment 0.05)

Fig. 2 Steady-flow performance of the sample rotor cascade with $\alpha_i = 40$ deg; $\alpha_o = -60$ deg; $M_i = 0.334$; and $M_o = 0.800$

static pressure fluctuations were typically between 4 and 4.5 percent of the average pressure. The corresponding values of V_{ip} for various values of V_{rb} were between 4.52 and 5.31 percent of c. For the results presented below we used $V_{ip} = 0.05\ c$. The following unsteady flow-field figures show that the potential-flow-interaction model inputs a sinusoidal static-pressure variation at the stator-exit/rotor-inlet computational boundary typical of that downstream of turbine cascades of various solidities, with a maximum value at the modeled stator trailing edge and a minimum value near the middle of the modeled line across the stator trailing edges.

The combined disturbance of the potential-flow and wake interactions are input as rotor-inlet distortions at the rotor-inlet computational boundary. This is done by adding the values of the two disturbances at that boundary, and by a coordinate transformation to the rotor-relative frame. These models include the effects of the stator potential-flow and wake

Table 1 Some information on the sample cascade

inlet flow angle α_i	40.00°
outlet flow angle α_o	−60.00°
stagger angle	−32.00°
loading coefficient C_L	0.80
cascade solidity S_{rb}/b_{rb}	0.6223
inlet Mach number M_i	0.334
outlet Mach number M_o	0.800
steady-flow x-force $F'_{x,ss}$	0.1140
steady-flow y-force $F'_{y,ss}$	0.1361
steady-flow z-moment $T'_{z,ss}$	0.0869
high nozzle angle α_N	74.49°
V_{rb} for high α_N	0.7026
$\tilde{\omega}$ for high α_N and $R = 2$	13.863
low nozzle angle α_N	66.75°
V_{rb} for low α_N	0.3783
$\tilde{\omega}$ for low α_N and $R = 2$	7.464

interactions on the rotor, and via the Euler solution in the rotor relative frame the effect of the rotor potential-flow field propagating upstream from the rotor leading-edge region to modify the potential-flow field in the axial gap between stator and rotor. They do not include the cross-coupling effect of the rotor potential-flow field modifying the (initial) stator potential-flow field.

Results

Wilson (1984) shows that a measure of cascade loading is the incompressible tangential-lift coefficient, given by:

$$C_L = 2\frac{S}{b}\cos^2\alpha_o[\tan(\alpha_i) - \tan(\alpha_o)] \tag{10}$$

For lightly, intermediately, and highly loaded cascades C_L is approximately 0.8, 1.0, and 1.2, respectively. Results have been obtained for numerous rotor cascades of various values of C_L and inlet and outlet flow angles. For discussion purposes we use a lightly loaded cascade designed with continuous-slope-of-curvature surfaces using the airfoil-design method (Korakianitis; 1987b, 1989). The sample cascade used in this study has incompressible tangential-lift coefficient $C_L = 0.80$. Its steady-flow performance is shown in Fig. 2. Additional information about this cascade is shown in Table 1. The relative amplitudes of the rotor-inlet flow distortions due to the potential-flow and wake interactions in each case are functions of the nozzle angle α_N and the corresponding rotor velocity V_{rb}. They can be computed using the information supplied in Table 1 to reconstruct the velocity diagram at the rotor-inlet boundary. The values for the forces $F'_{x,ss}$, $F'_{y,ss}$, and $T'_{x,ss}$ in Table 1 have been evaluated by running the unsteady-flow program with $D = 0.0$ and $V_{ip} = 0.0$ (the resulting "unsteady" performance is identical to the steady-flow performance shown in Fig. 2).

The wake and potential-flow were modeled at the rotor-inlet boundary as described above. The forces and moments were calculated under these conditions for two nozzle angles (corresponding to two identical rotor-relative velocity triangles, but different stator velocity triangles). As the rotor moves past a series of stator pitches, the forces and moment exhibit a periodic pattern. To investigate these patterns, we chose to

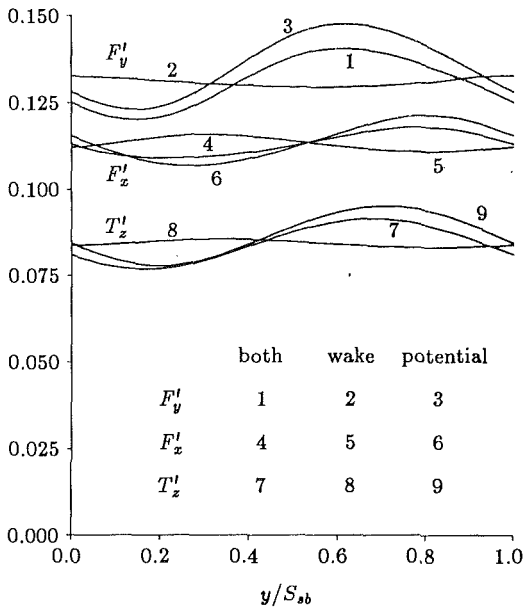

Fig. 3 Time evolution of the forces and moment over a full stator pitch for the high nozzle angle ($\alpha_N = 74.49$ deg)

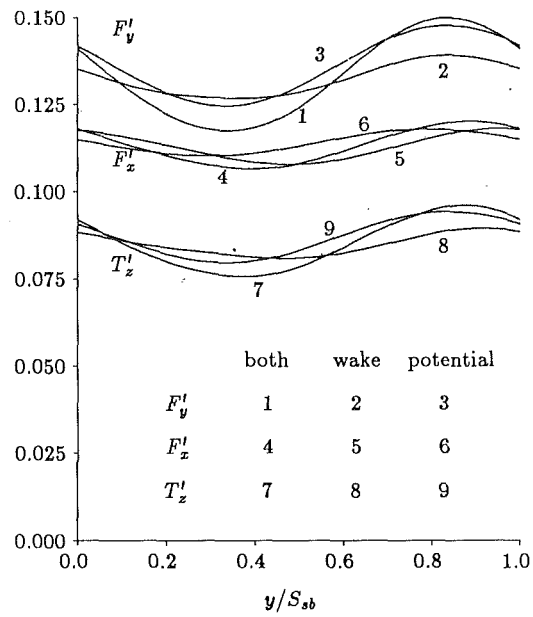

Fig. 4 Time evolution of the forces and moment over a full stator pitch for the low nozzle angle ($\alpha_N = 66.75$ deg)

study the effects of the wake and potential-flow interactions on the sample cascade moving past a stator that has double the pitch of the rotor ($R = 2$). In production engines designers would normally try to choose unequal integers for all blade rows, and R would not be an integer. This unlikely geometry is useful for the purposes of this paper because it provides a symmetry that facilitates the discussion (see later figures), because it is in a range where both types of interaction are of comparable magnitude (so that neither one dominates the generation of the unsteady part of the force (Korakianitis, 1987a, 1992a, 1992b)), and because it is close to the value of R of many turbine stages in production engines.

The origin ($t = y/S_{sb} = 0.0$) of the period of the unsteadiness in each case (Figs. 3, 4, 5, 6) corresponds to the y location at which a stator velocity wake touches the leading edge of a rotor blade (numbered blade 0 in the following figures). The end of the period ($t = y/S_{sb} = 1.0$) corresponds to the velocity wake from the next stator blade touching the leading edge of the same rotor blade. In each case we considered the interaction of the rotor blade row under three different conditions: (*a*) with the isolated potential-flow interaction (the wake amplitude D was set equal to zero); (*b*) with the isolated viscous-wake interaction (the potential amplitude V_{ip} was set equal to zero); and (*c*) with the combined interaction of the viscous-wake and potential-flow interactions. These studies can only be performed on a computer because in experimental or production turbine stages both types of interaction are always present.

The dimensional forces per unit length of blade span (such as F_x in the x direction) are related to the nondimensional forces (F'_x) by:

$$F'_x \equiv \frac{F_x/z}{\rho\, b_{rb}\, c^2} \tag{11}$$

(the moment T'_z is taken about the leading edge, and it is divided by b_{rb}^2).

Figures 3 and 4 show the unsteady part of the forces and moment for blade 0 over one stator pitch. To understand how these forces vary from the average value, we considered the propagation of the unsteady part of the pressure in the passages. The unsteady pressure at a point is defined as the instantaneous pressure at any time t minus the steady-flow pressure at that point. Because $R = 2$ the flow is repeating every other passage, and at $t = 0$ the next wake impinges at the leading edge of blade 2. This means that what occurs between blades 0 and 1 at $t = 0.50$ occurs between blades 1 and 2 at time $t = 0.00$. Thus for every figure shown at time $t = \tau$, we can also deduce the flow at time $t = \tau + 0.50$. (This was one of the reasons for which we chose $R = 2$ for discussion.) The unsteady pressure contours with increment 0.002 for the high nozzle angle and for times $t = 0.000$, [0.167], 0.333, [0.500], 0.667, and [0.833], for isolated potential-flow interaction, for the isolated wake interaction, and for the combined interaction are shown in Fig. 5. The square brackets indicate that one should consider the blades with numbers in square brackets in the appropriate plot. The corresponding unsteady pressure contours for the low nozzle angle are shown in Fig. 6. Entropy contours are superimposed to show the location of the velocity wake. The rotor is always shown at the same location; as time increases the wake and the potential-flow interaction of the stator are shown moving at the rotor-inlet boundary toward the negative Y values. The regions in which the unsteady pressure is positive are dotted. In the remaining regions the unsteady pressures are negative. Following the dotted or the not-dotted regions from their edge inward or outward, one can derive the values of the corresponding unsteady pressures anywhere in the flow field. In Figs. 5 and 6 the increment of the unsteady pressure contours is 1/10th of the increment of the steady-flow pressure contours shown in Fig. 2. The blades are numbered starting from blade 0, which is the blade at the leading edge of which the centerline of a wake impinges at time $t = 0$.

Discussion

The shape of F'_x, F'_y, and T'_z in Figs. 3 and 4 indicates that the spatially analyzed Fourier harmonics of the unsteady forces is dominated by the first harmonic amplitude, and that the amplitude of the second harmonic is an order of magnitude smaller than the first harmonic for $R = 2$. These agree with the conclusions from our past work. Higher values of wake defect D, velocity disturbances due to the potential V_{ip} or stator-to-rotor-pitch ratio R result in forcing functions with higher amplitudes for the second and third harmonics (Korakianitis, 1987a, 1988a, 1992b). The stator-outlet flow velocities V_N are

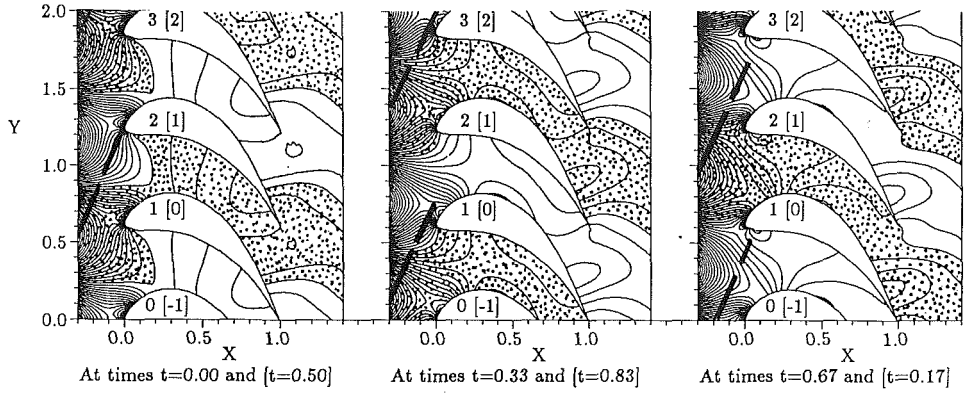

Fig. 5(*a*) Unsteady pressure contours (increment 0.002) for isolated potential-flow interaction

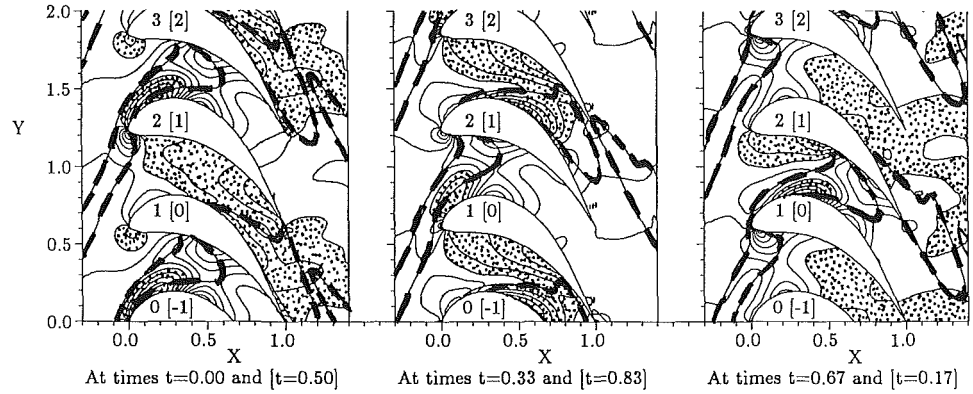

Fig. 5(*b*) Unsteady pressure contours (increment 0.002) for isolated viscous-wake interaction

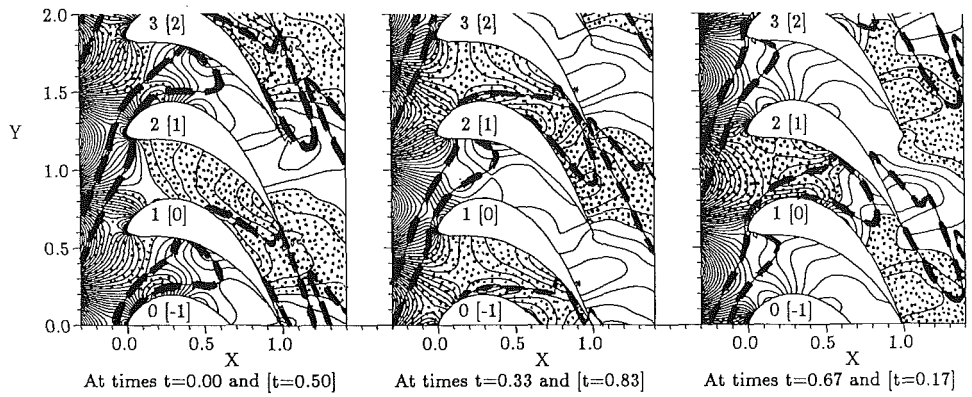

Fig. 5(*c*) Unsteady pressure contours increment 0.002 for the combined interaction

Fig. 5 Unsteady pressure contours of increment 0.002 showing the propagation of disturbances in cascade 4060c08 for high nozzle angle. Left, time $t=0$ and [$t=0.50$]. Middle $t=0.33$ and [$t=0.83$]. Right, $t=0.67$ and [$t=0.17$].

in the high subsonic regime in this paper. Higher velocities may induce shocks in the passages that will result in forcing functions with even higher harmonics (see the flow fields of Giles, 1990).

Potential-Flow Interaction. The explanation of the potential-flow interaction in this paper extends our previous interpretations, where we considered two limiting cases of rotor velocity (first infinitely small V_{rb}, and second a higher V_{rb} resulting in just subsonic flow fields) to show that the potential interaction originates at the rotor-inlet boundary and it is affected by the rotor velocity. Here we show some additional details of the temporal variation of the potential-flow interaction.

The effect of the potential-flow field of the stator on the potential-flow field of the rotor can be seen by the distortion (existence) of the unsteady pressure lines in Figs. 5(*a*) and 6(*a*). The effect of the potential-flow field of the rotor on the flow can be seen where the wake centerlines are bent near the leading edge of the rotors in Figs. 5(*b*) and 6(*b*). The initial directions of the wake centerlines are shown as dashed lines in Figs. 5(*a*) and 6(*a*) to indicate the location of the stators. The weaker potential flow field of the rotor blades cuts into the stronger and stationary potential flow field of the stators. Figures 5(*a*) and 6(*a*) show the positive unsteady pressure at the trailing edges of the stator, the negative unsteady pressure between the trailing edges of the stator, and the rapid decay of the potential-flow interaction downstream of the stator trailing edge. As the rotor passage moves it cuts the potential flow field of the stator into two regions: one upstream region, still attached to the stator; and one downstream region which is now traversing with the rotor. The latter propagates downstream superimposed on the rotor flow field according to potential-flow theory while continuously decaying. This can be seen in Fig. 5(*a*) between blades 0 and 1 (also corresponding to the passage between blades 2 and 3). At time $t=0$ the relative position of rotor and stator is such that a positive portion of the potential (called PPP) has moved into the rotor passage almost to the

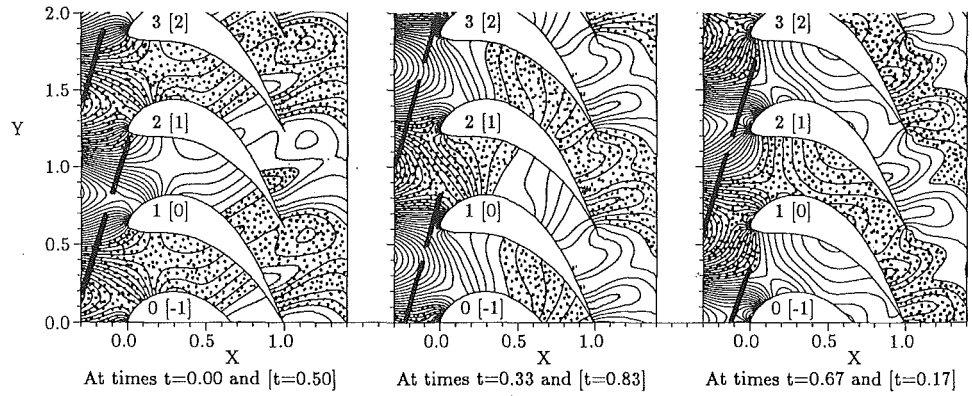

Fig. 6(*a*) Unsteady pressure contours (increment 0.002) for isolated potential-flow interaction

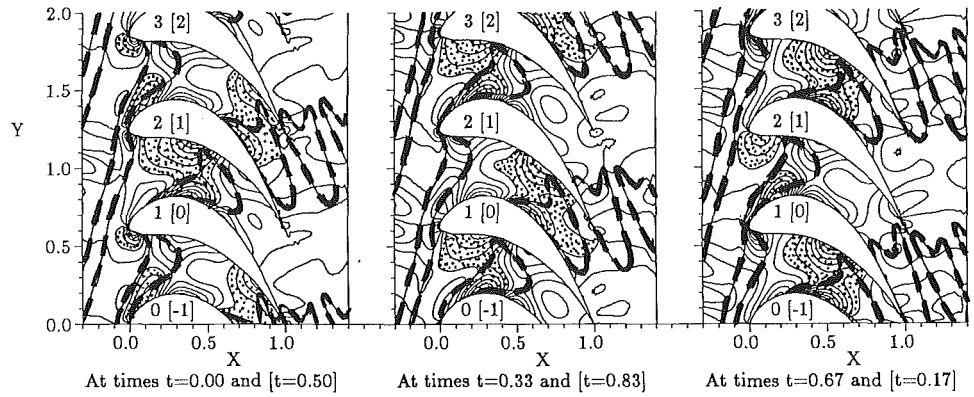

Fig. 6(*b*) Unsteady pressure contours (increment 0.002) for isolated viscous-wake interaction

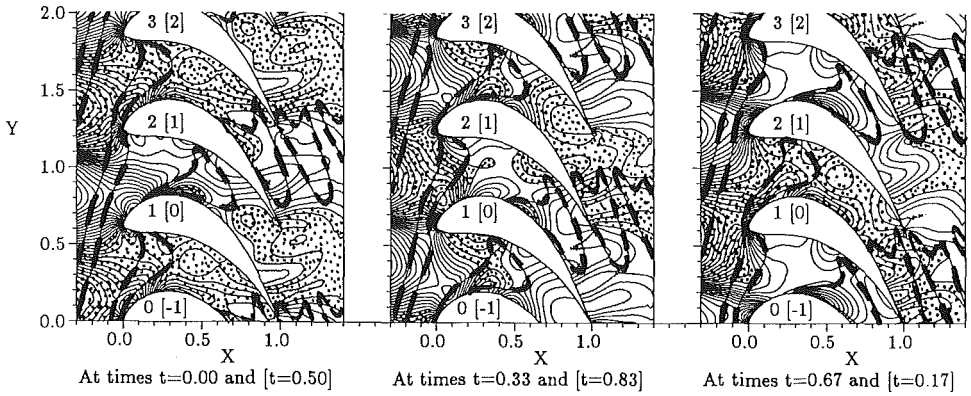

Fig. 6(*c*) Unsteady pressure contours (increment 0.002) for the combined interaction

Fig. 6 Unsteady pressure contours of increment 0.002 showing the propagation of disturbances in cascade 4060c08 for low nozzle angle. Left, time $t=0$ and [$t=0.50$]. Middle, $t=0.33$ and [$t=0.83$]. Right, $t=0.67$ and [$t=0.17$].

rotor throat. The shape and velocity of the rotor cascade passage distorts the potential-flow field. A similar negative portion of the potential (called NPP) has moved into the next passage between blades 1 and 2. At [$t=0.17$] the rotor leading edge has cut half of the PPP off, while the rotor-passage portion of the PPP has almost been separated from the inflow-boundary portion of the PPP, and part of it has moved into the rotor-outflow region. At time $t=0.33$ the PPP has moved past $X=0.5$ in the passage and even more of it is in the rotor-outflow region. At [$t=0.50$] it has reached the rotor throat. At times $t=0.67$ and [$t=0.83$] the first PPP is into the rotor outflow region and it has merged with the next portion of positive potential from the next stator trailing edge. Similar observations can be made for the low nozzle angle in Fig. 6(*a*). One can observe a direct correspondence between the space and time location of the maxima and minima in the unsteady pressure fields in Figs. 5(*a*) and 6(*a*), and the increases or decreases from the average forces in Figs. 3 and 4, respectively.

The potential-flow interaction from the stator extends into the rotor cascade passages and large portions of it enter the cascade when the direction of propagation of the potential is aimed near the center of the rotor passage (best illustrated at $t=0.67$ in Fig. 6*a*). The potential flow field of the stator is cut by the advancing potential flow field of the rotor (best illustrated at $t=0.00$ in Fig. 6*a*). After it is cut it moves downstream according to Eq. (7) as a potential-flow disturbance superimposed in the rotor flow field (best illustrated at all values of t in Fig. 5*a*).

Wake Interaction. The explanation of the wake interaction in this paper extends previous interpretations. Meyer (1958) and Lefcort (1965) considered the cutting of wakes by the rotor, and Smith (1966) introduced the idea of distinct wake segments in the rotor passages. Hodson (1985a) discussed the rotation of the cut wake segments and the effects of the lower momentum fluid in the wake region, and Korakianitis (1987a,

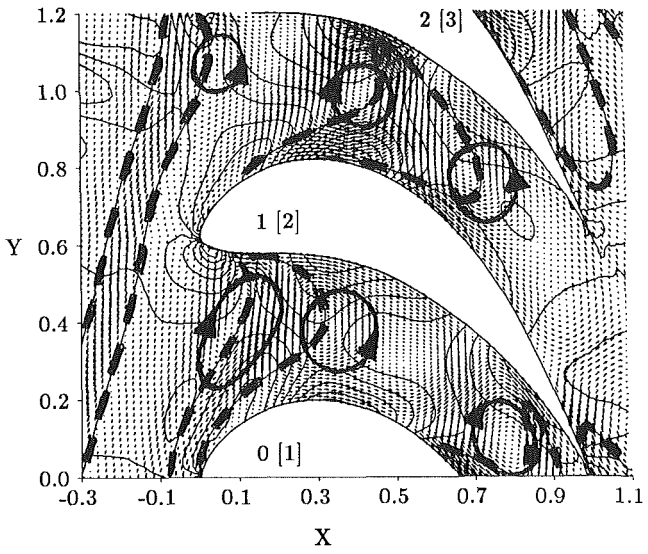

Fig. 7 Unsteady flow vectors of magnitude 0.45 superimposed on unsteady pressure contours of increment 0.002 and on entropy contours for the high nozzle angle at $t=0$

1988c, 1992b) used the idea of recirculating flows to show how they resulted in "suction" and "impingement" of unsteady-flow (low-momentum) jets that generate suction and pressure regions in the turbine passages. In Korakianitis (1992b) we stated that " . . . the temporal variation of these instantaneous pressure maxima and minima, which act in addition to the local pressure in steady flow, generate the unsteady forces on the blade . . . ". Here we show and explain some new and additional details of the temporal variation of the wake interaction.

The wake centerlines are shown as superimposed entropy contours in Figs. 5(b) and 6(b), respectively. We concentrate on a small region of Fig. 5b at time $t=0$, for $1.2>Y>0.0$. The unsteady flow vectors superimposed on entropy contours and unsteady pressure contours for that region are shown in Fig. 7. The unsteady flow vectors are defined as the instantaneous local velocity minus the local steady-flow velocity. The entropy contours locate the wake centerlines, and the positive and negative values of unsteady pressure can be found by comparing Figs. 5(b) and 7.

The wakes are first bent by the potential flow field of the rotor as shown in the region $(X, Y)=(-0.2, 0.7)$ in Fig. 7. As the leading edge in the rotor stagnation region interacts with the lower-momentum fluid in the wake (for example near points $(X, Y)=(0.0, 0.0)$ and $(X, Y)=(0.0, 1.2)$), recirculating-flow patterns are established in the stagnation region of the leading edge of the rotor as shown in the region $(X, Y)=(0.0, 1.1)$ in Fig. 7. These recirculating flow patterns are generated as the wake is being cut; once generated they result in a counterclockwise rotating unsteady-flow pattern downstream of the wake centerline, and a clockwise rotating unsteady-flow pattern upstream of the wake centerline. The wakes are cut by the passing rotor into individual segments that are acting in each passage. After the stator wake is cut to produce a segment of a wake in the rotor passage, the two ends of the wake segment travel at the local speeds: the portion attached to the pressure side moves downstream into the passage much slower than the portion attached to the suction side, because the local flow velocities are higher on the suction side of the cascade. At the same time lower momentum fluid moves from the wake end near the pressure side to the wake end near the suction side. The last two phenomena cause a thinner wake on the pressure side, a thicker wake on the suction side, and a counterclockwise rotation of the centerline of the wake as it moves through the passage. The initial vorticity is conserved; before the wake is cut, for example near $(X, Y)=(-0.3, 0.4)$ and $(X, Y)=(-0.2, 0.4)$, there is no unsteady pressure on either side of the wake; after the wake is cut, for example near $(X, Y)=(0.4, 1.0)$ and $(X, Y)=(0.7, 0.8)$ there is substantial positive unsteady pressure on the upstream side of the wake and negative unsteady pressure on the downstream side of the wake. These vortices start to form as the leading edge of the rotor shears into the downstream side of the wake, generating the positive unsteady pressures upstream of the wake centerline (for example near $(X, Y)=(0.05, 0.1)$ and $(X, Y)=(0.05, 0.6)$) and the negative unsteady pressures downstream of the wake centerline (for example near $(X, Y)=(0.05, 0.7)$ and $(X, Y)=(0.05, 1.2)$). The two counterrotating vortices that flank the wake centerline must be equal and opposite. The two vortex patterns act in opposite directions. The upstream clockwise-rotating vortical flow pattern causes a local increase in pressure, and the downstream counterclockwise-rotating vortical flow pattern causes a local decrease in pressure. As the vortices move downstream and out of the rotor cascade, the wake is sheared, distorted, and enlarged, while the amplitude of the unsteady pressure maximum or minimum is decreased and its region of influence increased. One can observe a direct correspondence between the space and time location of the maxima and minima in the unsteady pressure fields in Figs. 5(b) and 6(b), and the increases or decreases from the average forces in Figs. 3 and 4, respectively.

The cutting of the wake by the rotor generates two recirculating regions of low-momentum fluid, one upstream and the other downstream of the wake centerline. The unsteady forces from the wake interaction are due to the positive unsteady pressure (generated in the vortical pattern upstream of the wake centerline) and due to the negative unsteady pressure (generated in the vortical pattern downstream of the wake centerline).

Figures 5(b) and 6(b) indicate that the wakes from lower stator exit angles act for a shorter part of the period (actually of a triple period from blade 0 to blade 4 or 5) in the rotor cascade. The residence times of the wakes inside the rotor cascade are longer for the higher nozzle angles, but there are also better opportunities for unsteady pressure maxima (or minima) to align themselves at opposite sides of the blades and thus reduce the resultant unsteady force. The residence times inside the rotor cascade are shorter for the lower nozzle angles, but there are fewer opportunities for unsteady pressure maxima (or minima) to align themselves at opposite sides of the blades because their wakes also spread more in the axial direction of the cascade. It is more likely for an unsteady pressure maximum on one side to align with a minimum on the other side of the blade and maximize the unsteady force. The unsteady forces for the isolated wake interaction from lower values of nozzle angle are likely to be higher than those from higher values of nozzle angle. The forces in Figs. 3 and 4 and the unsteady pressure contours in Figs. 5(b) and 6(b) indicate that indeed this is the case for the sample cascade. Although many parameters affect the results (loading also plays an important role on the propagation of disturbances), this result is confirmed by observing the results from most similar loaded cascades associated with this and our past studies.

Combined Potential-Flow and Wake Interactions. The combination of both interactions is shown in Figs. 5(c) and 6(c). It is easier to study the effects of the combined interaction by first looking at Figs. 5(a) and 6(a), and at Figs. 5(b) and 6(b), and then considering Figs. 5(c) and 6(c). The corresponding unsteady pressure maxima and minima due to the combined interaction are easily interpreted as the combined (additive) effect of the two interactions described above. The

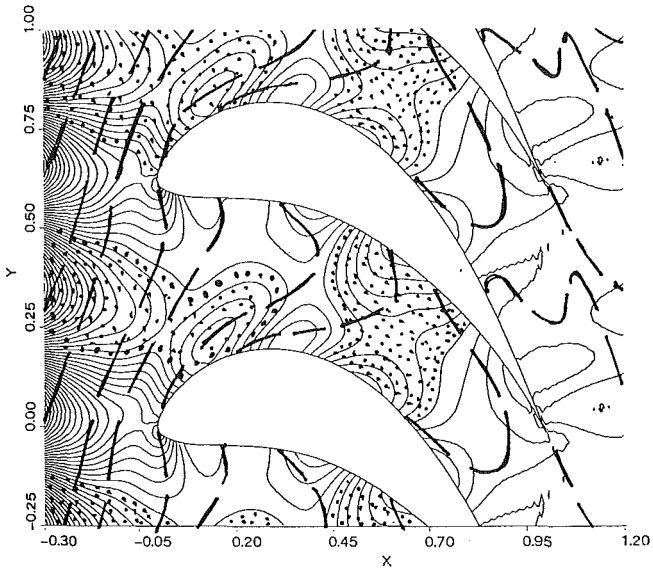

Fig. 8 Unsteady pressure contours of increment 0.002 from the combined interaction for $R=1$

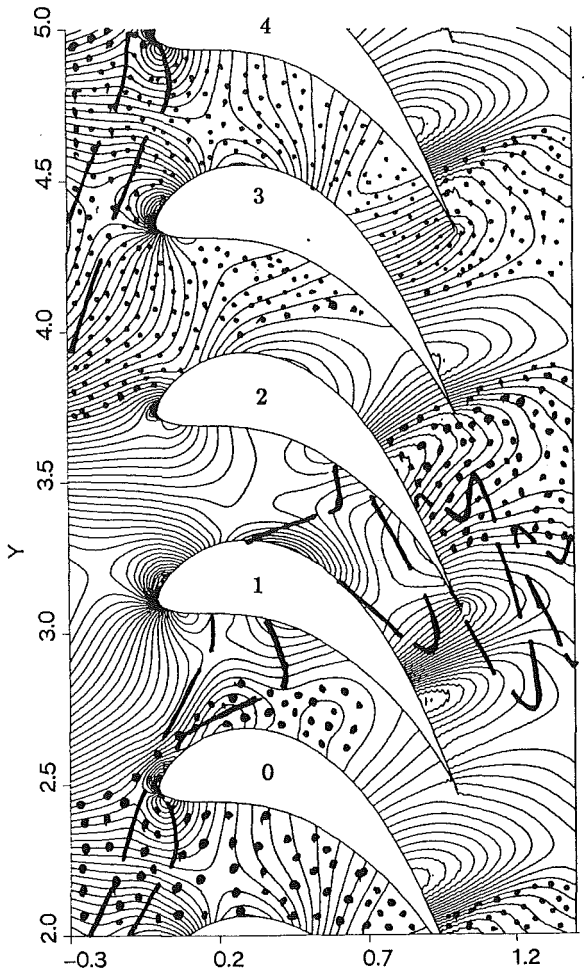

Fig. 9 Unsteady pressure contours of increment 0.002 from the combined interaction for $R=4$

magnitude of the unsteadiness of the force is increasing or decreasing accordingly at different times in Figs. 3 and 4. In general the unsteadiness in F_y' is lower for the high nozzle angle because of counteraction of the two disturbances (see Figs. 3 and 5), and higher for the low nozzle angle because of reinforcement of the two disturbances (see Figs. 4 and 6).

The value of R has a significant effect on which type of interaction dominates the unsteady flow field. Figure 8 shows the unsteady pressure contours and the entropy contours from the combined interaction for the same cascade and for a ratio $R=1$ at $t=0$. In this case the potential-flow interaction decays very fast downstream so that it hardly affects the flow in the rotor cascade. The unsteady pressure contours inside the cascade passage are due to the wake interaction only, and they agree with the explanation of the wake interaction discussed above. Figure 9 shows the unsteady pressure contours and the entropy contours from the combined interaction for the same cascade and for a ratio $R=4$ at $t=0$. In this case the potential flow interaction decays very slowly downstream and it dominates the flow in the rotor cascade. The unsteady pressure contours due to the wake interaction are visible only above blade 0. The region of positive unsteady pressure downstream of blade 2 is also due to the potential-flow interaction.

Conclusions

The unsteady forces on two-dimensional gas-turbine rotors due to potential-flow and viscous-wake interactions from upstream blade rows are computed using a compressible, two-dimensional, inviscid rotor/stator-disturbance interaction program. The viscous wake and the potential-flow interactions from the upstream stator are modeled as inlet distortions at the rotor-inlet boundary. New explanations of the mechanism of generation of unsteady forces on turbine blades are offered by observing unsteady pressure contours in the rotor passages. The results used in this paper to facilitate the discussion have been compared with the results from numerous other cascades of a variety of loading distributions and geometries. The conclusions presented in this paper have been confirmed by all cases we have studied to date.

We conclude the following:

1 The potential flow field of the rotor cuts into the potential flow field of the stator and vice versa. After the potential flow disturbance from the stator is cut into a rotor cascade, it propagates into the relative flow field of the rotor passage as a potential-flow disturbance superimposed on the rotor flow field. Due to the relative size of rotor and stator, the unsteadiness from the potential flow field dominates the rotor flow field only at high values of R.

2 The potential flow field of the rotor near the leading edge and the leading edge itself cut into the wake. The cutting action generates two counterrotating vortical patterns flanking the wake-segment centerline in the passage. The vortical pattern upstream of the wake centerline generates an increase in local pressure (and forces acting on the sides of the passage). The vortical pattern downstream of the wake centerline generates a decrease in local pressure (and forces acting on the sides of the passage). The wake-segment ends attached to the sides of the passage travel at the local flow velocities; the wake-segment end near the suction surface moves downstream faster than the wake-segment end near the pressure surface; and the centerline of the wake segment rotates counterclockwise as it propagates downstream. Due to the relative size of rotor and stator, the unsteadiness from the vortex patterns generated by the wake dominate the rotor flow field at low values of R.

3 The unsteady forces on the blades due to the potential-flow and wake interactions acting simultaneously are generated by the combined (additive) interaction of the two disturbances. The unsteady pressure fields due to the combined interaction can be explained by considering the influence of each type of interaction in different regions of the flow.

4 For low values of stator-to-rotor-pitch ratio ($R \approx 1$) the

unsteady forces are dominated by the wake interaction. For high values of stator-to-rotor-pitch ratio ($R > 3$) the unsteady forces are dominated by the potential-flow interaction. For intermediate values of stator-to-rotor-pitch ratio ($R \approx 2$) the unsteady forces are affected by both wake interaction and potential-flow interaction.

Acknowledgments

The author thanks Professor Michael B. Giles and Rolls Royce plc. for their permission to use UNSFLO in this investigation, and the Department of Mechanical Engineering at Washington University in St. Louis for supporting his work on this research program.

References

Binder, A., Forster, W., Mach, K., and Rogge, H., 1987, "Unsteady Flow Interaction Caused by Stator Secondary Vortices in a Turbine Rotor," ASME JOURNAL OF TURBOMACHINERY, Vol. 109, pp. 251–257.

Boletis, E., and Sieverding, C. H., 1984, "Experimental Study of the Flow Field Behind an Annular Turbine Nozzle Guide Vane With and Without Downstream Rotor," ASME Paper No. 84-GT-15.

Giles, M. B., 1988a, "Calculation of Unsteady Wake/Rotor-Interactions," *AIAA Journal of Propulsion and Power*, Vol. 4, pp. 356–362.

Giles, M. B., 1988b, "UNSFLO: A Numerical Method for Unsteady Inviscid Flow in Turbomachinery," MIT Gas Turbine Laboratory Report No. 195, Oct.

Giles, M. B., 1990, "Stator/Rotor Interaction in a Transonic Turbine," *AIAA Journal of Propulsion and Power*, Vol. 6, pp. 621–627.

Gostelow, J. P., 1984, *Cascade Aerodynamics*, Pergamon Press, New York.

Hodson, H. P., 1983, "Unsteady Boundary-Layers on Axial-Flow Turbine Rotor Blades," PhD thesis, University of Cambridge, United Kingdom.

Hodson, H. P., 1985a, "An Inviscid Blade-to-Blade Prediction of a Wake-Generated Unsteady Flow," ASME *Journal of Engineering for Gas Turbines and Power*, Vol. 107, pp. 337–344.

Hodson, H. P., 1985b, "Measurements of Wake-Generated Unsteadiness in the Rotor Passages of Axial Flow Turbines," ASME *Journal of Engineering for Gas Turbines and Power*, Vol. 107, pp. 467–476.

Korakianitis, T., 1987a, "A Design Method for the Prediction of Unsteady Forces on Subsonic, Axial Gas-Turbine Blades," Doctoral thesis (Sc.D.) in Mechanical Engineering, Massachusetts Institute of Technology, Cambridge, MA.

Korakianitis, T., 1987b, "A Parametric Method for Direct Gas-Turbine-Blade Design," AIAA Paper No. 87-2171.

Korakianitis, T., and Wilson, D. G., 1988a, "The Effect of the Magnitude of the Inlet-Boundary Disturbance on the Unsteady Forces on Axial Gas-Turbine Blades," *Proceedings of the Fourth International Symposium on Unsteady Aerodynamics and Aeroelasticity of Turbomachines and Propellers*, Aachen, Sept. 6–10, 1987, H. E. Gallus and S. Servaty, eds., published by RWTH Aachen, Feb. 1988, pp. 109–124.

Korakianitis, T., 1988b, "On the Prediction of Unsteady Forces on Gas Turbine Blades. Part 1: Typical Results and Potential-Flow-Interaction Effects," ASME Paper No. 88-GT-89.

Korakianitis, T., 1988c, "On the Prediction of Unsteady Forces on Gas Turbine Blades. Part 2: Viscous-Wake-Interaction and Axial-Gap Effects," ASME Paper No. 88-GT-90.

Korakianitis, T., 1989, "Design of Airfoils and Cascades of Airfoils," *AIAA Journal*, Vol. 27, No. 4, pp 455–461.

Korakianitis, T., 1992a, "On the Prediction of Unsteady Forces on Gas Turbine Blades. Part 1: Description of the Approach," ASME JOURNAL OF TURBOMACHINERY, Vol. 114, pp. 114–122.

Korakianitis, T., 1992b, "On the Prediction of Unsteady Forces on Gas Turbine Blades. Part 2: Analysis of the Results," ASME JOURNAL OF TURBOMACHINERY Vol. 114, pp. 123–131.

Lefcort, M. D., 1965, "An Investigation of Unsteady Blade Forces in Turbomachines," ASME *Journal of Engineering for Power*, Vol. 87, pp. 345–354.

Liepmann, H. W., and Roshko, A., 1957, *Elements of Gasdynamics*, Wiley, New York.

Meyer, R. X., 1958, "The Effect of Wakes on the Transient Pressure and Velocity Distributions in Turbomachines," *Trans. ASME*, Vol. 80, pp. 1544–1552.

Sieverding, C. H., Van Hove, W., and Boletis, E., 1984, "Experimental Study of the Three-Dimensional Flow Field in an Annular Turbine Nozzle Guide Vane," ASME *Journal of Engineering for Gas Turbines and Power*, Vol. 106, pp. 437–448.

Smith, L. H., 1966, "Wake Dispersion in Turbomachines," ASME *Journal of Basic Engineering*, Vol. 88, pp. 688–690.

Sonoda, T., 1985, "Experimental Investigation of Spatial Development of Streamwise Vortices in a Turbine Inlet Guide Vane Cascade," ASME Paper No. 85-GT-20.

Wilson, D. G., 1984, *The Design of High-Efficiency Turbomachinery and Gas Turbines*, The MIT Press, Cambridge, MA.

Yamamoto, A., and Yanagi, R., 1985, "Production and Development of Secondary Flows and Losses Within a Three Dimensional Turbine," ASME Paper No. 85-GT-217.